J. Appl. Comput. Mech., xx(x) (2026) 1-13
DOI: 10.22055/jacm.2026.49121.5747

ISSN: 2383-4536
jacm.scu.ac.ir

Shahid Chamran University of Ahvaz

Journal of Applied and Computational Mechanics

Research Paper

Machine Learning Modeling and Experimental Optimization of Heat Exchanger for Efficient Building Systems

Nayeemuddin Mohammed[1], Faizan Ahmed[2], Hiren Mewada[3]

[1] Department of Civil Engineering, Prince Mohammad Bin Fahd University, Al Khobar, Saudi Arabia, Email: mnayeemuddin@pmu.edu.sa

[2] Department of Mechanical Engineering, Prince Mohammad Bin Fahd University, Al Khobar, Saudi Arabia, Email: fahmed@pmu.edu.sa

[3] Department of Electrical Engineering, Prince Mohammad Bin Fahd University, Al Khobar, Saudi Arabia, Email: hmewada@pmu.edu.sa

Received February 01 2026; Revised April 29 2026; Accepted for publication May 01 2026.
✉ Corresponding author: N. Mohammed (mnayeemuddin@pmu.edu.sa)

Abstract. The compact design, high thermal efficiency, and adaptability to various fluids make plate heat exchangers (PHE) valuable applications in smart buildings. A computer-controlled experimentation unit employs PLC-SCADA software to monitor and record fluid temperature, flow rate, enabling efficient control, visualization, and data recording. The experimental results indicate the hot and cold fluid flow rate 0.5-1.4 l/min, 1-3 l/min, feed temperature (50–60 °C), optimal heat exchanger efficiency 58.54 %. Response Surface Methodology (RSM) and Machine Learning (ML) such as Decision Tree (DT), Adaptive Boosting (AdaBoost), and Bootstrap Aggregating (Bagging) were used along with hyperparameters using grid search to achieve the best predictive performance. RSM demonstrates the highest accuracy, achieving an R^2 of 0.99 and low error metrics (RMSE = 0.71, MAE = 0.62), making it a robust method for performance prediction. Bagging demonstrated the best performance, with an R^2 score of 0.942 and 0.935 on the training and test datasets, the lowest error (RMSE = 2.037, MAE = 1.566) on the test dataset. To link the algorithm's predictions to thermal physics, a feature-importance analysis using Shapley Additive Explanations (SHAP) is also conducted. It is observed that the cold fluid flow rate is the primary driving parameter for prediction, showing an inverse relationship with effectiveness. The findings of this research indicate that both RSM and ML techniques can predict the PHE effectiveness with good accuracy. This paper proposes a key experimental and data-driven approach for predicting and optimizing the performance of a PHE that can be integrated into smart building technologies.

Keywords: Machine learning, Modeling, Optimization, Heat exchanger, Effectiveness.

1. Introduction

Plate heat exchangers (PHE) are useful in a variety of applications such as energy generation, chemical, manufacturing, food technology, and air conditioning due to their high thermal efficiency, versatility, and ease of cleaning [1]. A PHE consists of a stack of metal plates that are tightly sealed [2]. The flow distribution of the hot and cold streams is governed by the plate perforations and gasket designs, thereby creating numerous narrow channels between the plates [3]. PHE is flexible, maintainable, and has superior heat-transfer properties compared with shell-and-tube pattern heat exchangers [4]. They have a larger surface area and a smaller hydraulic diameter, offering better thermal and hydraulic performance [5]. However, due to design and operational factors, as well as interactions among the input variables, predicting and optimizing PHE performance becomes difficult. Besides being resource-intensive, traditional approaches often fail to account for the interaction effects among input parameters.

To this extent, some scientists studied thermal and hydrodynamic properties in a two-channel chevron-style heat exchanger. They investigated the Nusselt number and the friction factor in both turbulent and laminar environments. Although the results demonstrate efficacy consistent with conventional counter-flow, the temperature distributions showed distorted isothermal patterns influenced by the channel shape [6]. In another study, a significant increase in the convective heat transfer coefficient, specific heat capacity, and thermal conductivity was observed when nanofluids were employed in PHE. In addition, graphene-based nanofluid exhibited 24.7% increase in efficiency when compared to titanium oxide-based nanofluid [7]. In one study, the use of a magnetic field decreased effectiveness by 15%. This was attributed to high nanoparticle concentration (1%). Hence, the nanoparticle composition and magnetic field characteristics need to be optimized for effective PHE operation [8]. Similarly, some scholars examined the stagnation point flow of hybrid nanofluids over a plate with convective, suction, and radiation barrier effects. They reported that increasing the fraction of nanoparticles increases the friction on the skin and decreases the Nusselt number. However, the suction increases the friction and heat transfer while reducing the temperature. Response surface methods indicate that optimal suction, Biot number, and radiation yield the maximum Nusselt number [9]. Compared to metal heat exchangers, polymer

Published online: May 08 2026

heat exchangers are less expensive and more corrosion resistant. However, new research indicates that aluminum performs similarly when dry. Despite this, polymers are used in consumer appliances like dehumidifiers and dryers due to their strength and ease of production [10]. Another study reported that increasing the flow channels resulted in flow maldistribution. Although downstream swirl flow compensates for velocity and temperature distributions, computational data indicate that outlet points have higher flow, whereas inlet points have lower flow [11]. Similarly, in another study, the heat transmission coefficient remained constant at the higher flow rates. No trends were observed for heat transmission at temperatures up to 550 °C, which was likely due to thermal expansion affecting the heat exchanger [12]. Another study optimized the mass fraction and temperature of aqueous ionic liquids. The thermal conductivity, viscosity and specific heat capacity were enhanced under optimal conditions for solar energy applications [13].

Numerous studies are focusing on enhancing the performance of PHE by examining new design configurations [14]. Most approaches enhance PHE design by reducing the heat-transfer area while maintaining constraints on channel, pressure drop, and flow velocity [15]. One study investigated sustainable optimization of PHE with undulating surfaces [16]. The study utilized computational fluid dynamics for optimization. Correlations were developed for the friction factor and the Nusselt number, yielding an ideal design over a range of flow rates [17]. The thermal effectiveness was reported to be enhanced by 13% in another study that employed computational fluid dynamics modeling. It also improved flow homogeneity by decreasing maldistribution by 47% in the laminar pattern and 24% in the turbulent pattern. The pressure drop was found to decrease by 56.9% [18]. Another scholar developed an adsorption-based PHE absorber for thermal storage and cooling applications. The experimental and computational evaluations showed significantly superior adsorption kinetics and a 310% increase in water absorption when compared to traditional coated exchangers. The improved performance under typical operating conditions was verified using a 3D coupled heat-and-mass transport model [19].

Some scientists have reviewed and summarized the applications of machine learning in heat exchanger modeling for design optimization. They demonstrated that machine learning is a powerful tool for modeling the performance of heat exchangers [20]. Likewise, other scientists investigated the thermal and flow characteristics of crossflow heat exchangers with helical fins. It was reported that the Reynolds number affects heat transfer. Air velocity was the primary factor increasing heat transfer. In addition, combining artificial neural networks with RSM resulted in high prediction accuracy for the Nusselt number and the friction factor. Further progress may be made by focusing on artificial intelligence-based optimization and advanced computational methods [21]. He et al. [22] studied a rapid surrogate model developed to predict fouling in industrial heat exchangers, using steam generators in nuclear power plants as a case study to enable efficient performance assessment. Yang et al. [23] proposed a real-time, high-accuracy optimization under varying constraints, significantly improving computational efficiency and enabling practical application in rapid microchannel heat sink design.

Despite extensive research on PHE, most current studies use either ML approaches for predictive modeling or RSM alone for statistical optimization. RSM is effective in detecting parameter interactions, but the prediction accuracy is poor. Moreover, ML models are good at predicting but lack the interpretability and systematic design framework of RSM. The combination of RSM and ML methods for analysis of the PHE was only partially explored. This leaves a gap in the development of a comprehensive framework combining predictive robustness and optimization capabilities. Inspired by this gap, the current work aims to leverage the predictive power of ML while capturing parametric interactions with the statistical rigor of RSM.

In this study, we use RSM-BBD to investigate the influence of critical operating factors on the thermal performance of plate-mounted heat exchanger. Several experiments were performed using the BBD matrix and a regression model was then developed to predict the efficacy of PHE. Optimal factor settings are reported. In addition, models are developed using three machine learning techniques: DT, AdaBoost and Baggage. The root mean square error (RMSE), mean absolute error (MAE), mean squared error (MSE) and coefficient of determination (R^2) have been calculated and a detailed comparison of the proposed models is presented. In addition, an analysis of the importance of features is performed to identify key driving parameters in machine learning models. These data-driven methods are a productive replacement for fault detection, energy efficiency control and real-time forecasting in heat systems using heat exchangers on the plate. One of the objectives of this study is to identify key factors and their relationship to optimizing PHE performance. Another objective is to provide a reliable and robust framework for predicting the performance of the PHE in the context of the development of smart building technologies.

2. Methodology

2.1. Experimental facility

The arrangement of the experimental unit is depicted in Fig. 1. The experimental facility comprises three units: the auxiliary unit, the heat exchanger unit, and the computer interface unit. The auxiliary units consist of a water-heating tank, flow sensors, flow-regulation valves, and a hot-water pump. The heat exchanger unit comprises a series of parallel steel plates assembled together to form the plate heat exchanger. The space between any two adjacent plates creates a channel through which the fluid flows. Hot and cold fluids pass along alternate zones inside the heat exchanger. Heat exchanger occurs through the actual plate boundary separating the two fluids. This module also includes four temperature sensors to measure the exit and inlet temperatures of the cold and hot fluids as they pass through the heat exchanger. The computer interface unit consists of data monitoring and recording of both fluid temperatures and flow rates. This unit features PLC-SCADA software that allows for efficient process control, visualization and data recording. Figure 2 illustrates the process of heat and fluid flow. The specifications of the base unit are provided in Table 1, and those of the plate heat exchanger are listed in Table 2.

Table 1. Base unit.

Sr No.	Item	Specification
1	Flow Valves	6 valves
2	Control valve	0.7 bar (maximum pressure)
3	Pump	0 - 3 l/min
4	Tank	Stainless Steel, 30-liter, 3000 W (input)
5	Flow sensors	2 sensors, Range: 0 - 7 l/min, Accuracy: ±1.25%
6	Connecting tubes	4 tubes

Table 2. Plate heat exchanger.

Sr No.	Parameter	Specification
1	Plate spacing	2 mm
2	Total plates	20 (280 x 100 mm, each plate)
3	Plate material	Stainless steel
4	Dimensions	500 x 300 x 100 mm
5	Valves	4 valves
6	Thermocouples	J-Type, 4 sensors, Range: 0 - 600 °C, Accuracy: ± 1.75 °C
7	Surface area	0.64 m^2
8	Diameter (port)	30 mm

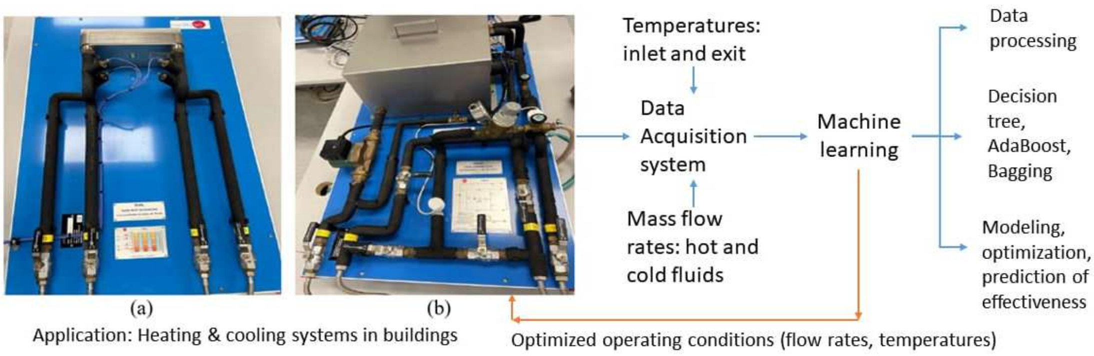

Fig. 1. Experimental facility, (a) Heat exchanger (b) Base unit.

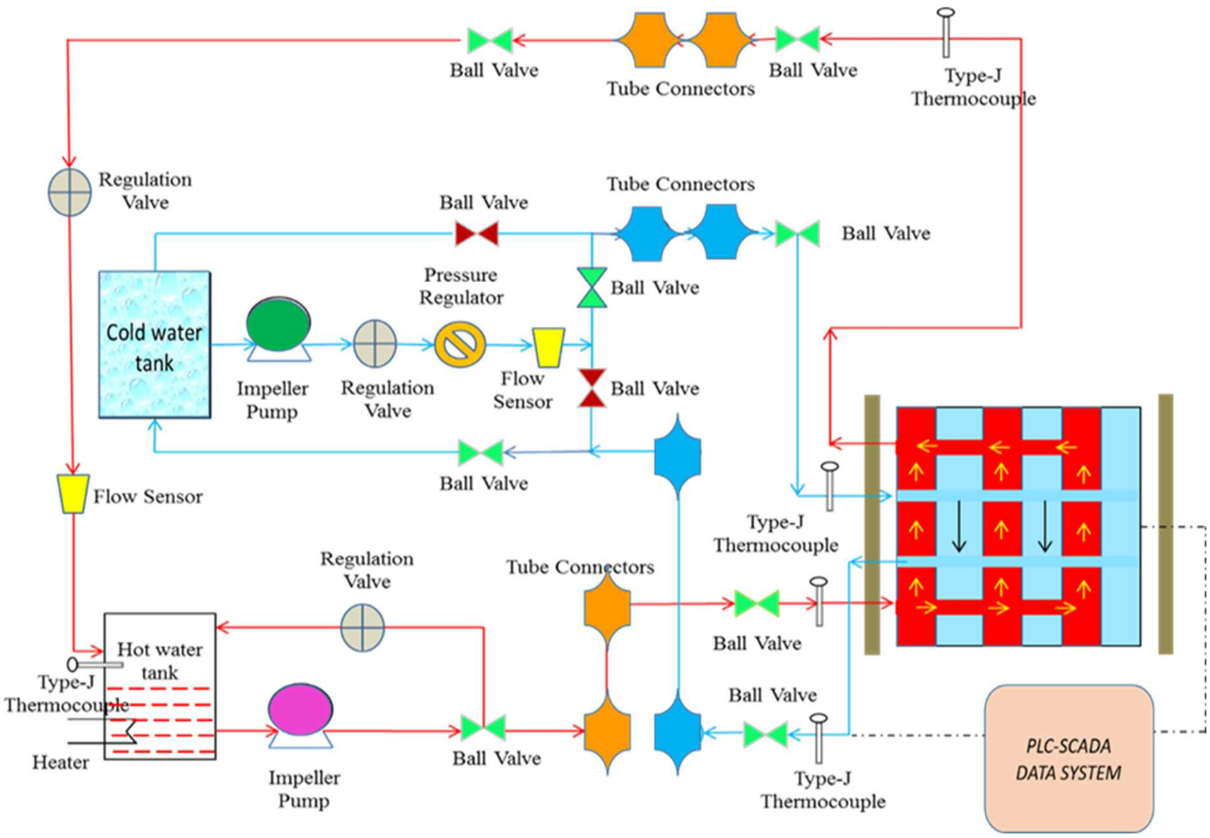

Fig. 2. Schematic of experimental setup.

System operation and experimentation begin by heating the hot fluid in the heating tank to the desired temperature. This heating is achieved using a resistance heating element. Next, the heated water is pumped into the heat exchanger by an impeller pump. Similarly, the cold fluid is forced into the heat exchanger from another storage tank. As both fluids enter the heat exchanger, they exchange heat through the plates separating them. As a result, the hot fluid releases heat, and the cold fluid gains heat after the heat exchange. Experiments were carried out at various input settings, namely, hot-fluid inlet temperature and hot- and cold-fluid flow rates. The entry and exit temperatures of cold and hot fluids are recorded and subsequently, the heat exchanger efficiency is obtained for each test case.

2.2. Response surface methodology-box Behnken design

Figure 3 illustrates the steps involved in Box Behnken Design. BBD is a successful experimental design technique for process optimization and prediction. It fits a second-order (quadratic) model to experimental data. Compared to other RSM designs, such as Central Composite Design, Box Behnken Design requires fewer experimental runs because it uses only three levels per factor and does not test extreme axial points [24]. In situations where testing high- or low-level extremes is either physically impossible or expensive [25]. BBD enables the effective fitting of second-order models while avoiding impractical operating conditions or introducing uncertainty, thereby providing high-quality data within the operating region of interest. While Central Composite Design (CCD) might improve the ability to extrapolate because of axial points, the goal of this work is to predict within the experimental range; in addition, as machine learning models are empirical, the quality and physical meaning of the data are more important for prediction than coverage of the design. In addition, it enables testing at mid-edge points and the center area [26]. In the proposed RSM-BBD experimental model, experiments with three center points were developed as per Eq. (1):

$$N = 2k(k-1) + C_0 \tag{1}$$

where, N is the number of experimental runs, k is the number of factors, and C_0 is the number of centers. The general second-order quadratic polynomial equation [27] used to predict the response is presented in Eq. (2):

$$Y = \beta_0 + \sum_{i=1}^{k} \beta_i X_i + \sum_{i=1}^{k} \beta_{ii} X_i^2 + \sum_{i<j}^{k} \beta_{ij} X_i X_j + \varepsilon \tag{2}$$

where, Y is the prediction for the response, β_0 is the constant term, β_i is the linear coefficient, β_{ii} is the quadratic coefficient, β_{ij} is the interaction coefficient, $X_i X_j$ is the coded independent variable, ε is the random error.

2.3. Machine learning models

(a) AdaBoost machine learning algorithm

Adaptive Boosting is a common ensemble learning technique employed to improve the performance of weak signal processors. AdaBoost works by gradually training a series of low-level learners, often in Decision Tree form, each one focusing on the previous mistakes [28]. This method assigns weights to each training instance, increasing the weight of incorrectly classified examples and prompting successful classifiers to focus more on difficult situations. The model is generated by aggregating all the predictions of the weak learners weighted by their performance. This adaptive method reduces bias and variability, leading to greater accuracy for both the training and the unknown data. AdaBoost is particularly effective for binary classification tasks and has been successfully used in various areas, including image recognition and text classification, due to its robustness and noise-free data handling capabilities. Figure 4 presents the flow chart of the AdaBoost machine learning technique.

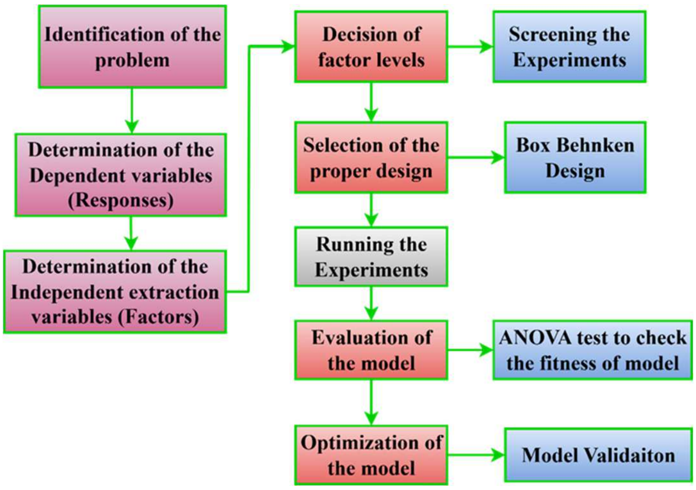

Fig. 3. Flowchart of Box Behnken design for optimization.

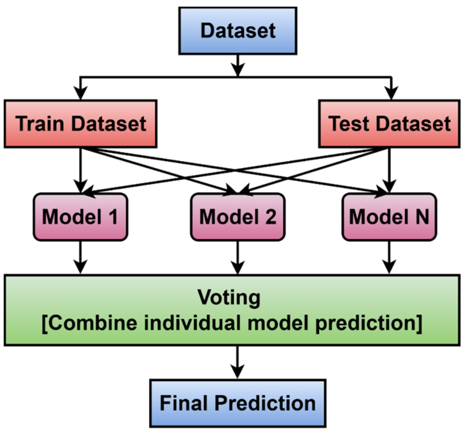

Fig. 4. Flowchart of the AdaBoost machine learning technique.

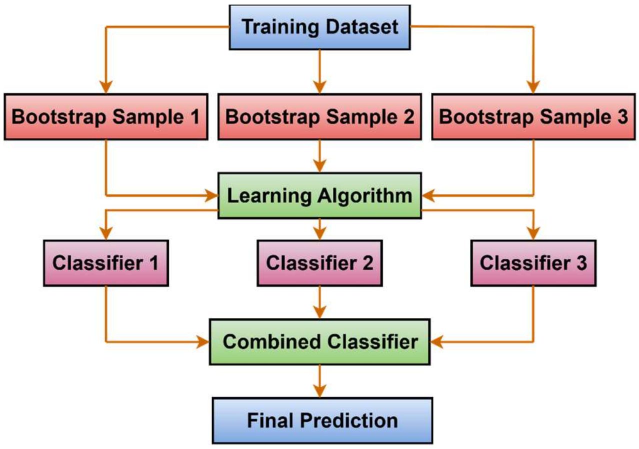

Fig. 5. Flowchart of the bagging machine learning technique.

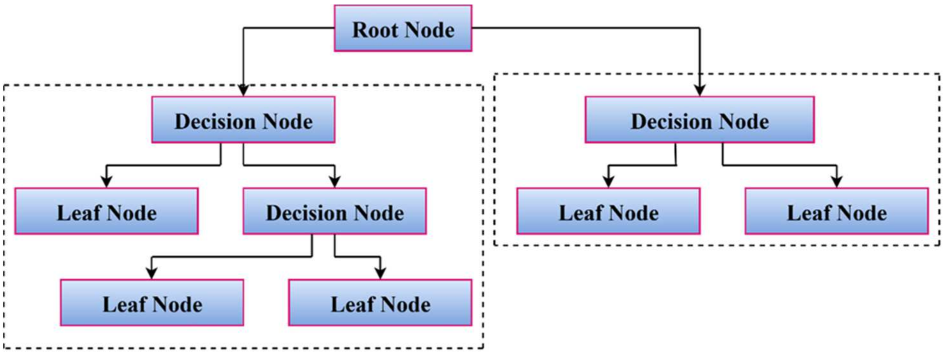

Fig. 6. Flowchart of the AdaBoost machine learning technique.

(b) Bagging machine learning algorithm

Bagging is a learning strategy that uses a number of ensembles to stabilize machine learning models [29]. Bagging aims to reduce variance and avoid overfitting by averaging the predictions of many base learning models, usually decision trees. It is a good method when the underlying model is very heterogeneous, as in the case of decision trees. It begins by Bootstrapping the training data set into subsets and training individual models on each subset. This aggregation smooths the errors of individual models and yields a more robust final forecast. Since decision trees are highly heterogeneous, bagging is a popular technique in practice for improving model performance and for enhancing the ensemble's interpretability, which can illuminate the overall decision process. Figure 5 illustrates the flowchart of the bagging method in machine learning.

(c) Decision tree machine learning algorithm

Decision trees are supervised machine learning algorithms that recursively partition the input space into regions of similar target values [30]. This partitioning is done by identifying the feature that best splits the dataset at each node, based on the impurity measure. The process repeats until the stopping criteria are met, such as the maximum depth or minimum number of samples per leaf. Figure 6 illustrates the flow chart of the Decision Tree machine learning technique.

Equations (3) to (7) were used in the metric analysis to identify the error values for various models:

- Mean Square Error:

$$\mathrm{MSE} = \frac{1}{n}\sum_{i=1}^{n}(y_i - \widehat{y_i})^2 \tag{3}$$

- Root Mean Square Error:

$$\mathrm{RMSE} = \sqrt{\frac{1}{n}\sum_{i=1}^{n}(y_i - \widehat{y_i})^2} \tag{4}$$

- Error Mean:

$$\mu_e = \frac{1}{n}\sum_{i=1}^{n}(y_i - \widehat{y_i}) \tag{5}$$

- Standard Deviation:

$$\sigma_e = \sqrt{\frac{1}{n-1}\sum_{i=1}^{n}[(y_i - \widehat{y_i}) - \mu_e]^2} \tag{6}$$

- Mean Absolute Error:

$$\mathrm{MAE} = \frac{1}{n}\sum_{i=1}^{n}|y_i - \widehat{y_i}| \tag{7}$$

Table 3. ANOVA analysis for effectiveness.

Source	Sum of Squares	df	Mean Square	F-Value	p-value	Remarks
Model	1227.13	9	136.35	87.74	< 0.0001	Significant
A-Hot flow rate	224.19	1	224.19	144.27	< 0.0001	
B-Cold flow rate	430.86	1	430.86	277.27	< 0.0001	
C-Inlet temp.	191.49	1	191.49	123.23	0.0001	
A^2	261.12	1	261.12	168.04	< 0.0001	
B^2	139.18	1	139.18	89.57	0.0001	
Residual	7.77	5	1.55			
Lack of Fit	7.47	3	2.49	16.64	0.0572	Not Significant

where, y_i is the actual value, $\widehat{y_i}$ is the predicted value, n is the number of sample data sets, σ_e is the standard deviation, μ_e is the error mean. Equation (8) represents the heat exchanger effectiveness. However, based on the properties of the hot and cold fluid, Eq. (9) or Eq. (10) serves for the computation of the plate heat exchanger effectiveness:

$$\varepsilon = \frac{Q_{actual}}{Q_{maximum}} \tag{8}$$

If $m_h C_{p,h} < m_c C_{p,c}$:

$$\varepsilon = \frac{T_{hi} - T_{ho}}{T_{hi} - T_{ci}} \tag{9}$$

If $m_c C_{p,c} < m_h C_{p,h}$:

$$\varepsilon = \frac{T_{co} - T_{ci}}{T_{hi} - T_{ci}} \tag{10}$$

where, Q is the heat transmission, W, ε is the effectiveness, m_h is the flow rate (hot fluid), kg/s, m_c is the flow rate (cold fluid), kg/s, $C_{p,h}$ is the specific heat (hot fluid), J/kgK, $C_{p,c}$ is the specific heat (cold fluid), J/kgK, T_{hi} is the inlet temperature (hot fluid), °C, T_{ci} is the inlet temperature (cold fluid), °C, T_{ho} is the exit temperature (hot fluid), °C, T_{co} is the exit temperature (cold fluid), °C.

3. Results and Discussion

3.1. RSM-based Box Behnken design

According to the results of the RSM-BBD experimental model, the Model F-value of 87.74 indicates that the model is significant, as there is only a 0.01% chance that an F-value this large would occur by chance. The p-values are all less than 0.0001, suggesting that terms A, B, C, A^2 and B^2 have a statistically significant effect on the response. Also, terms with p-values greater than 0.1000 may be removed from the model as they are not significant. The lack of fit F value of 16.64 and p-value of 5.72 indicate that the data is not fit and that refinement of the model may be justified, although it is often desirable that the lack of fit p-value is less than 10.0, as illustrated in Table 3.

The signal-to-noise ratio is measured by adequate precision. A value greater than 4 is the ideal ratio. The adequate signal is obtained as 30.677. The design space can be navigated using this model. For specific levels of each factor, predictions regarding the response can be made using the equation expressed in terms of coded factors. By default, the factors' high and low levels are denoted by the numbers +1 and -1, respectively. By comparing the factor coefficients, the model can determine the factor's relative impacts. Equation (11) represents the effectiveness in terms of coded factors, while Eq. (12) represents the effectiveness in terms of actual values of factors:

$$Y = 30.22 + 5.29A - 7.34B - 4.89C + 8.41A^2 + 6.14B^2 \tag{11}$$

$$Y = 378.03058 - 54.69640A - 39.86736B - 9.21089C + 41.52881A^2 + 6.13958B^2 \tag{12}$$

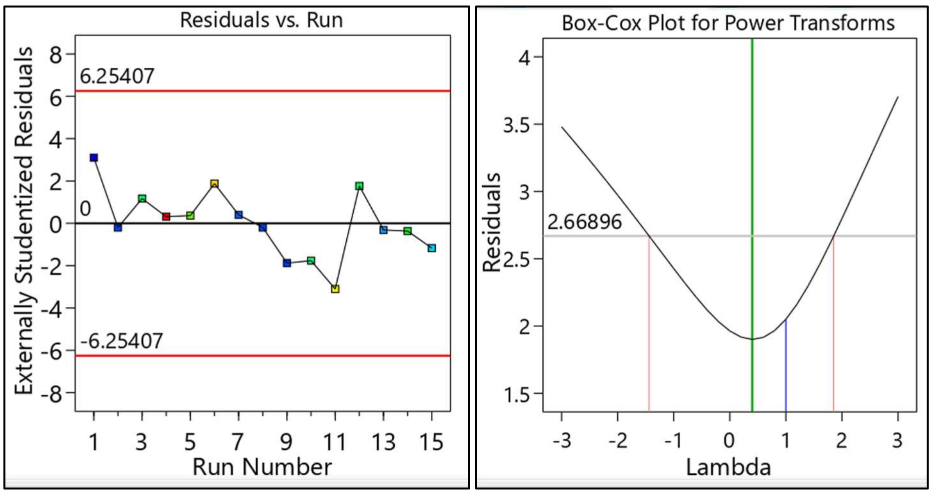

Fig. 7. Variation of residuals with runs and Box-Cox plot for the response.

The plot of externally studentized residuals versus run and the Box-Cox plot as indicated in Fig. 7. All the externally studentized residuals are within ±6.254, which is much smaller than 6.5 times the critical value. Therefore, there are no extreme outliers, and the residuals appear to be randomly scattered around zero, with no apparent pattern in their behavior across experimental runs. This implies that there is no systematic drift or time-related bias. Also, there is no violation of the independence assumption. The positive and negative values are balanced, indicating stability in the experimental procedure and in the fitted model being used to describe the data. The Box-Cox power transformation plot shown in Fig. 8 was used to assess whether changing the response variable would improve the model's adequacy. In this method, the transformation parameter, such as residual sum of squares, is estimated by applying the Box-Cox transformation. The curve represents the log-likelihood function for different values of 'lambda'. The vertical line indicates the estimated optimal value of the variable, and the two vertical lines indicate the 95% confidence interval. The horizontal line represents the upper limit of the confidence interval for the residual values. In this case, the optimal value of the parameter is approximately 1. The confidence interval includes the value 1 for the parameter, indicating that no transformation of the response is required [31]. This confirms that the model residuals meet the assumptions of normality and homogeneity of variance without requiring any transformation.

Figure 8 depicts the 2D contour and 3D surface plots enabling the visualization of the relationship between the dependent and independent variables. The contour plots are the topographic map of contour lines. The contour lines facilitate the identification of maximum or optimal regions and response variations between the factor variables. In addition, a 3D surface plot helps identify interaction effects between the input and output variables. The contour plots and the response surface reveal a strong nonlinear interaction between hot flow rate (A) and cold flow rate (B) on the heat exchanger's effectiveness. The higher the hot flow rate, the greater the effectiveness, especially when the cold flow rate is low, and it peaks at over 50%. This is explained by increased convective heat transfer on the hot side due to the higher Reynolds number, which promotes turbulence and increases the heat transfer coefficient. On the other hand, increasing the cold flow rate decreases effectiveness. Despite the increased convective heat transfer with higher cold-side flow, the rate of heat capacity also increases, thereby reducing the temperature increase of the cold fluid and the overall thermal driving force. This results in reduced actual-to-maximum heat transfer. The contour plot shows that the best performance occurs at high hot-flow rates and low cold-flow rates, where there is a balance between turbulence enhancement and thermal residence time. The elliptical shapes indicate that the second-order interaction between the variables is significant, as in the quadratic RSM model. In general, the observed trends are consistent with classical heat transfer theory, which demonstrates the interplay between Reynolds number and heat capacity rate on exchanger effectiveness.

Figure 9 displays the ramp plot of the best optimal solution. The numerical optimization results reveal that the optimal operating conditions were at a hot flow rate of 1.384 l/min, a cold flow rate of 1.0 l/min, and an inlet temperature of 53.968 °C. The response, which yielded an effectiveness of 58.54% and a desirability value of 1.0 (i.e., the overall desirability was 1.0, indicating that the chosen factor levels were optimal for all optimization criteria), was the first-ranked solution among the 100 feasible solutions generated.

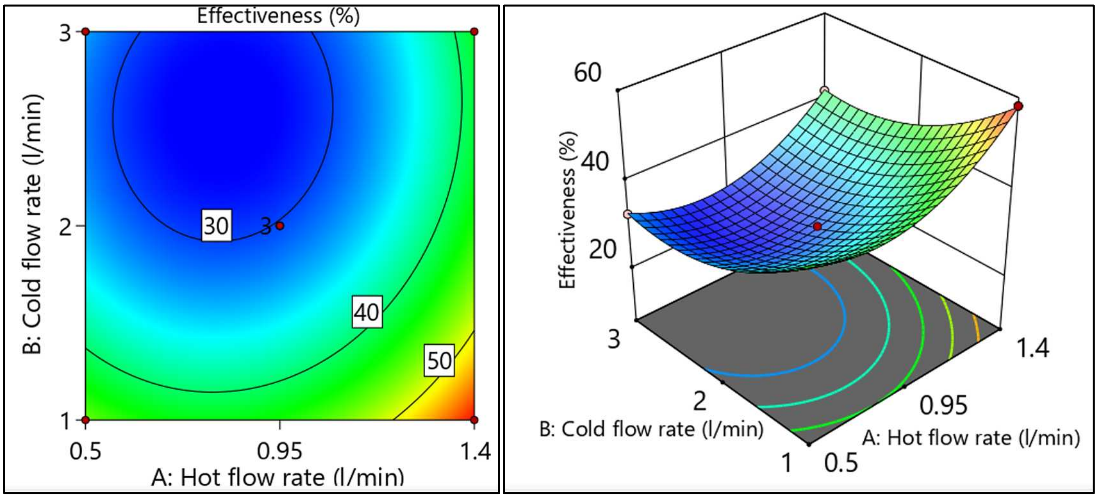

Fig. 8. Contour and 3D surface plot for the response.

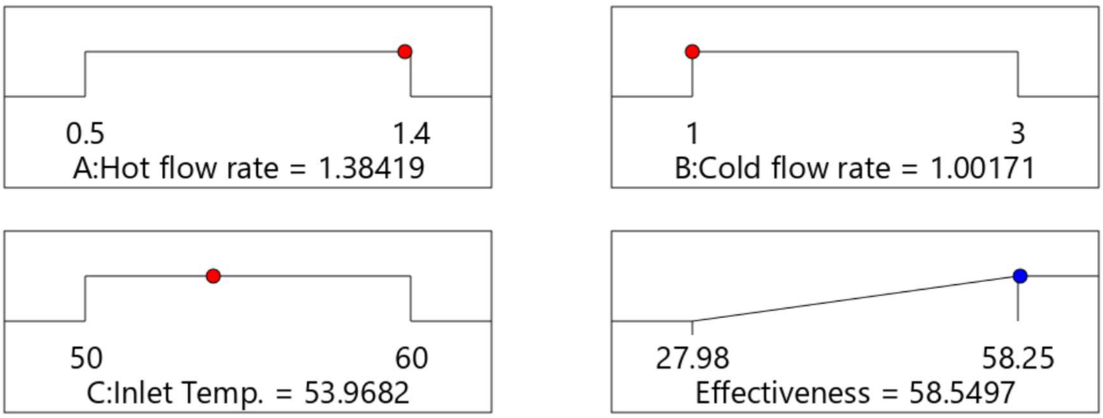

Fig. 9. Ramp plot of optimization.

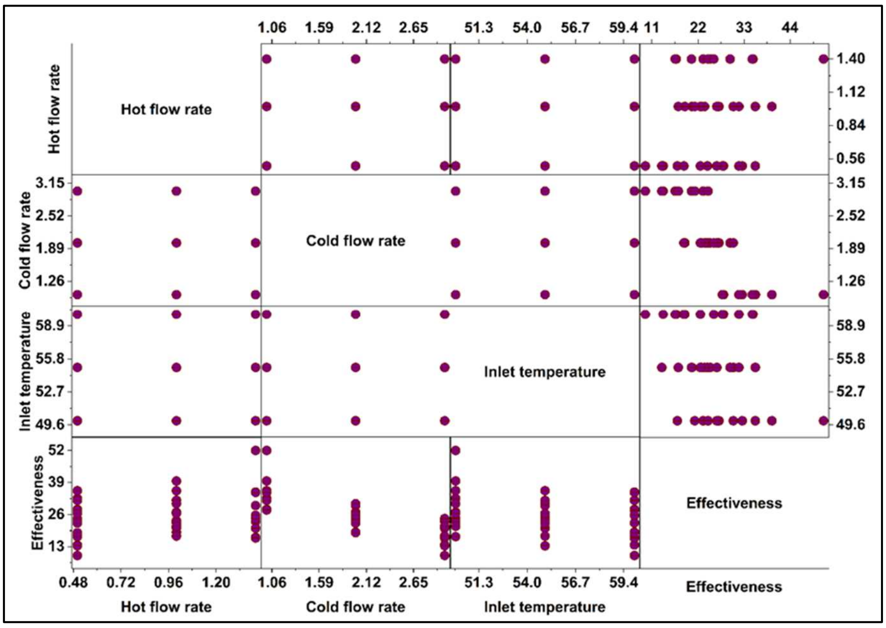

Fig. 10. Scatter plot for the input and output parameters.

3.2. Machine Learning model performance

The scatter plot matrix is illustrated in Fig. 10. The effects of operational parameters, such as input temperature, hot flow rate, and cold flow rate, on system efficiency are shown. The grouping is evident for each variable based on the distributional patterns, which is consistent with the structured nature of the experimental design [32]. The hot and cold flow rates are distributed across multiple levels to illustrate the regulated changes in these variables. The inlet temperature values are spread over a discrete set of points to ensure even coverage of the design space. The effectiveness values are found to cluster within a narrow range, suggesting that system performance is relatively stable across different operating conditions.

(a) Model parameter optimization using grid search with cross-validation (GrCV)

ML models are prone to overfitting if they are not well-tuned. Therefore, finding the optimum hyperparameter value is challenging. We systematically refine the hyperparameters of all three models using a grid-search-based cross-validation approach. GrCV finds the combination of hyperparameters that minimizes the model's prediction error while maintaining universality on unseen datasets. GrCV is a non-biased search algorithm that explores all possible combinations of hyperparameters for each model. Additionally, a 5-fold strategy, compared to a manual train-test split, rotates the data between training and test samples. The final score, i.e., MSE, is obtained by averaging all scores at all five folds. This ensures that the model is robust and not biased to specific data values. The tuning process for the three models used a 5-fold cross-validation strategy, and the following optimal parameters were identified. For the DT model, the maximum depth and minimum number of samples per leaf are optimized. AdaBoost performance depends on the number of estimators and the learning rate, whereas the number of estimators, maximum samples, and features are the three main hyperparameters for the Bagging method. Table 4 lists the range of these hyperparameters, and the corresponding optimum value obtained using GrCV is also presented

(b) Predictive performance and residual analysis

The predictive performance of the ML was initially evaluated by comparing predicted effectiveness values with measured effectiveness. The main analysis is residual analysis, which involves comparing observed and predicted values. Figure 11 shows performance during the training and testing phases using the decision tree machine learning technique. The upper panel illustrates the well-predicted values (outputs) compared with the actual target values for 10 sample indices. The prediction tracks the targets well, though there were minor fluctuations in a few cases. The MSE and RMSE values of 5.7866 and 2.4055, respectively, for the test data, indicate that the DT model provides a relatively good fit with low error variance. The histogram of errors and its fitted probability density curve show that the mean (–0.157) and standard deviation (2.5302) indicate a symmetric distribution around zero, with no significant prediction bias. These results demonstrate that the DT technique captures the trend in the underlying data reasonably well with acceptable generalization accuracy [33].

Figure 12 shows the AdaBoost predictions for the training and test datasets. The prediction error ranges from -4 to 4 for the training data and from -5 to 4 for the test data, respectively. The effectiveness value ranges from 13 to 51.96. The RMSE values of 2.04 and 2.87 indicate that predicted values deviate by 5.2% and 7.4% relative to this experimental span for the training and test data, respectively.

Table 4. Hyperparameter ranges and their optimal values using the GrCV method.

Model	Parameter	Range	Optimum Value
Decision tree	Max depth	[3, 5, 7]	5
	Minimum samples leaf	[1, 2, 3]	1
AdaBoost	Number of estimators	[50, 100, 150]	50
	Learning rate	[0.001, 0.01, 0.1]	0.01
Bagging model	Number of estimators	[50, 100, 150]	150
	Maximum samples	[0.6, 0.8, 1.0]	1
	Maximum features	[0.6, 0.8, 1.0]	0.8

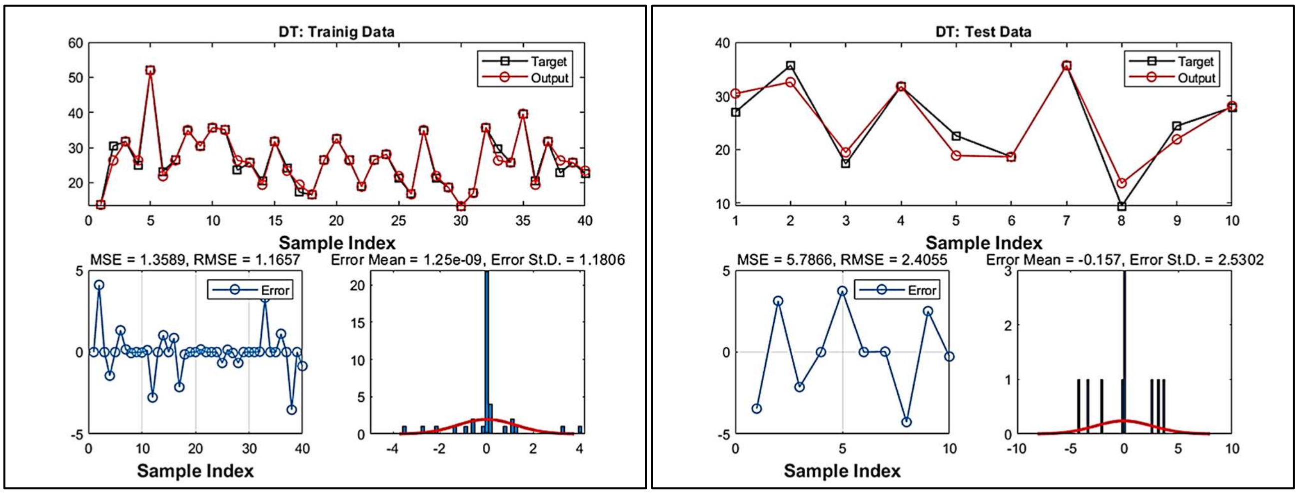

Fig. 11. Decision Tree-based results for training dataset and test dataset.

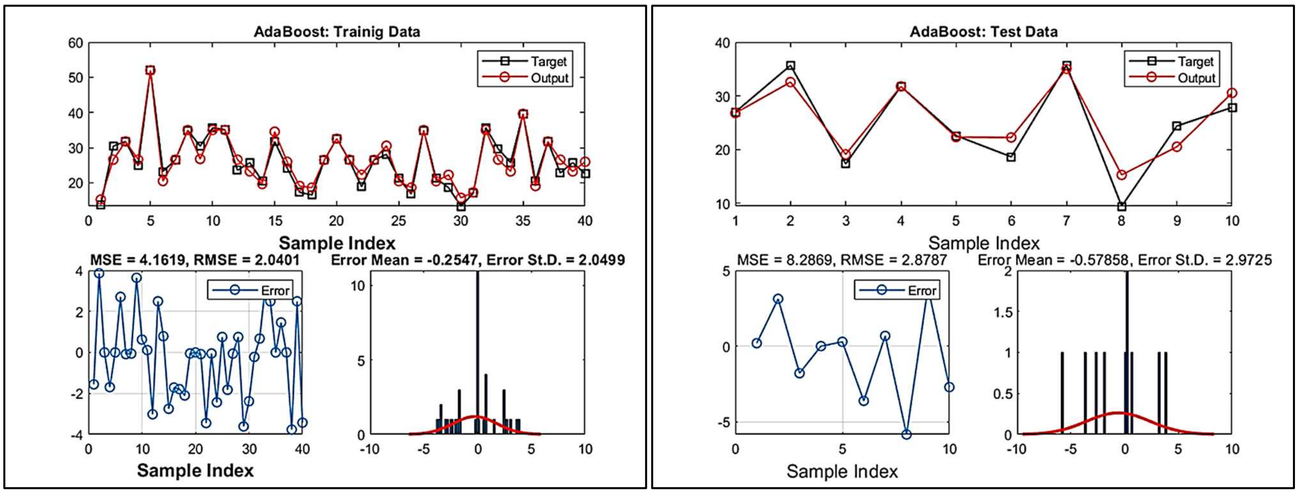

Fig. 12. AdaBoost-based results for training dataset and test dataset.

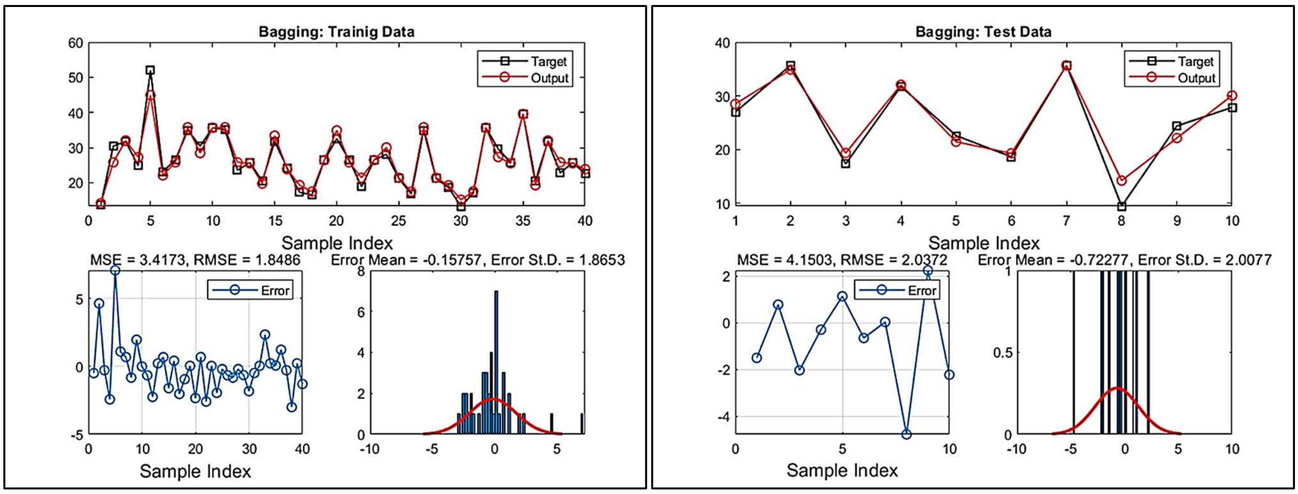

Fig. 13. Bagging-based results for training dataset and test dataset.

The predicted values and residual analysis using the Bagging method are presented in Fig. 13. The Bagging method performed best, with the lowest error among all ML algorithms. The reduction in training RMSE from 2.04 (AdaBoost) to 1.84 (Bagging) represents a 9.8% improvement in predictive precision. for training and test data. The Bagging model showed a significant improvement in generalization. It achieved an RMSE of 2.03 on the test dataset, which is 29.3% reduction compared to the 2.87 RMSE observed for the AdaBoost model on the same test set. AdaBoost is an iterative method, and Bagging utilizes an aggregation approach. The average of multiple trees may filter out outliers well and therefore achieve the lowest prediction error. Furthermore, the error gap between the training and test data predictions is smaller than that of AdaBoost and DT. This indicates that Bagging is more stable in the heat exchanger's effectiveness range.

(c) Statistical robustness and correlation assessment

The R^2 score is a statistical parameter that quantifies the proportion of variance in the Heat Exchanger Effectiveness explained by the model. To assess the ML's capability to predict and couple model performance with deterministic logic, this section presents a comparison of R^2 scores among three models, as shown in Fig. 14. The regression plots for DT are shown in Fig. 14(a) to evaluate the performance of the response variable. The R^2 values were 0.9771 for training and 0.9076 for testing, corresponding to about 97% and 90% of variance in the target values, respectively. This is considered a reasonable fit, but with some systematic bias towards overestimating the lowest actual value. Though DT achieved the largest R^2 Score among all, the test R^2 score is deviated by 0.07, suggesting some overfitting in the model. The AdaBoost achieved R^2 scores of 0.9313 and 0.8616, as shown in Fig. 14(b). The model has a compact cloud around the identity line, with an R^2 of 0.9313 on the training split. The residual spread appears roughly homoscedastic in the central range of 18 to 40, with no visible curvature. This indicates that AdaBoost is more sensitive to the outliers and, therefore, there is an issue of overfitting, resulting in a relative reduction in correlation stability.

In contrast, the Bagging algorithm is found to be robust for both training and test data, as shown in Fig. 14(c). It achieved an R^2 score of 0.9411 and maintained 0.9280 on the test dataset. There is a marginal deviation of 0.013 between the training and test phases. Thus, the Bagging model preserved 92.8% of the explained variance on unseen data. This demonstrates its superior ability to capture the fundamental thermal laws governing heat exchanger effectiveness. The measurement of a heat exchanger often contains fluctuations due to sensor sensitivity, transient flow turbulence, or minor ambient temperature changes. AdaBoost and Decision Tree are sensitive to these outliers. The use of parallel aggregation in the Bagging model smooths out these outliers well and allows the model to focus on the physical laws.

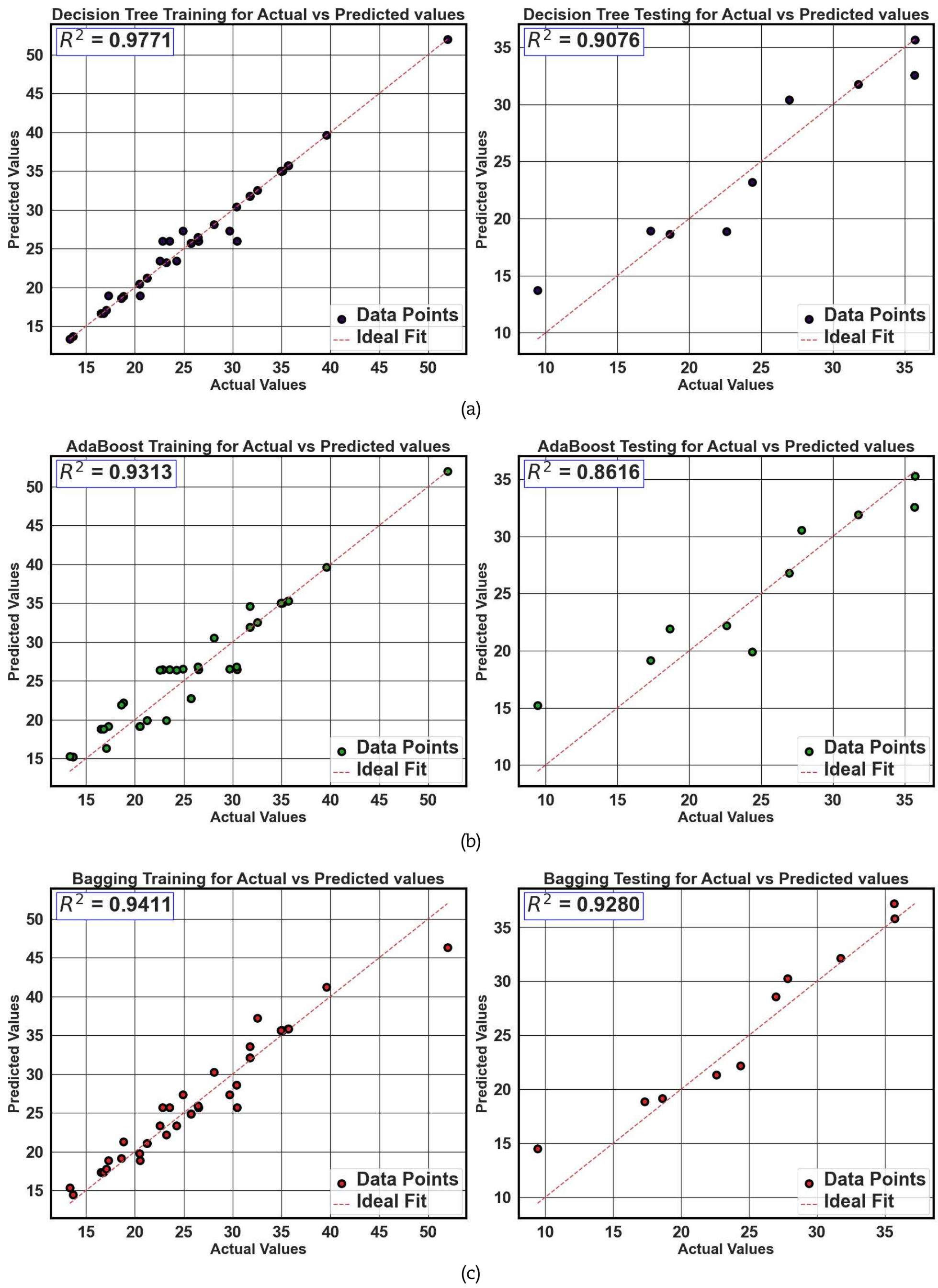

Fig. 14. R^2 Score analysis for (a) DT, (b) AdaBoost, and (c) Bagging.

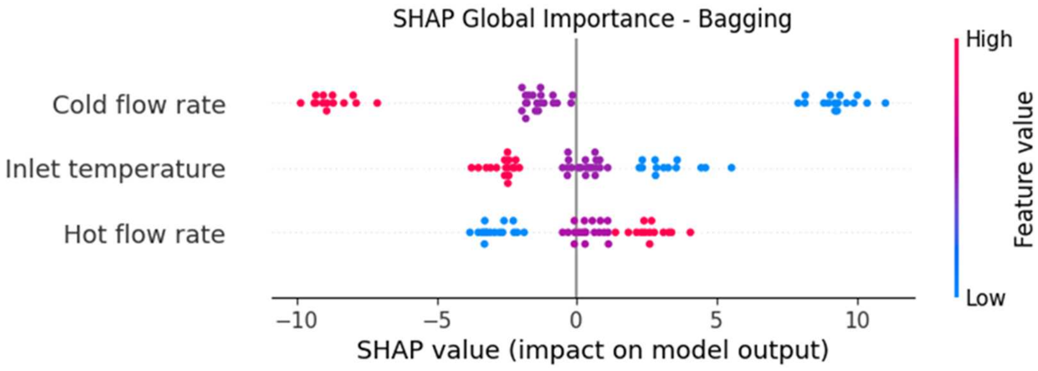

Fig. 15. SHAP analysis and input parameter ranking.

3.3. Input parameter importance using SHAP analysis and physical logic coupling

The model behaves as a black box in the prediction stage. To understand these models' behavior and verify their alignment with fundamental thermodynamic principles, a SHAP analysis is conducted on the input parameters. SHAP analysis finds the contribution of these three input parameters to the output. Figure 15 shows the SHAP values obtained using a highly performant model, i.e., Bagging. The SHAP value for a specific input is calculated by analyzing the model's performance when the input parameter is added, forming various combinations with other input parameters. The algorithm generates all possible combinations of cold flow rate, hot flow rate and input temperature. For each combination, calculate the difference in expected efficiency when the property (e.g. cold flow rate) is present or absent. These differences shall be averaged over all possible permutations in order to ensure that the contribution is equitable and reflects the interaction of the elements. The final forecast shall be the average efficiency for all samples plus the SHAP values for all inputs.

It states that the cold flow rate is the major contributor among the three, with inverse correlation. The lower flow rate has a positive impact on effectiveness. This is exactly consistent with physics, as lower flow velocities allow for longer thermal contact time, thereby enhancing heat-transfer recovery. The high concentration (red points) for the inlet temperature shows a consistent downward pressure on effectiveness. It is aligned with the expected reduction in thermal potential as the system approaches equilibrium. The hot flow rate is secondary in ranking, but statistically, it plays a significant role in predicting effectiveness. Increasing the hot flow rate increases the Reynolds number on the hot side of the exchanger. This causes a higher convective heat transfer coefficient and a reduction in overall thermal resistance. Thus, it may improve the total heat transfer rate and effectiveness. The lower ranking in SHAP analysis suggests that although the hot flow rate is a necessary parameter for optimization, its effectiveness is more sensitive to changes in the cold-side residence time than to changes in the hot-side convective strength. Overall, the input parameter ranking and their directional impacts are consistent with convective heat transfer governing equations. This confirms that ML model predictions are fundamentally aligned with physics.

4. Conclusion

This investigation examined the experimental optimization and ML-based modeling of a heat exchanger for smart building applications. The critical operation factors, cold flow rate, hot flow rate, and inlet temperature, are examined well by employing RSM-BBD. The optimal heat exchanger effectiveness was determined to be 58.54%. The numerical optimization results reveal the optimal operating conditions were at a hot flow rate of 1.384 l/min, a cold flow rate of 1.0 l/min, and an inlet temperature of 53.968°C. Later, three advanced ML models were used to surpass the limitations of traditional polynomial regression. The statistical performance, as assessed by residual and correlation analyses, showed that the Bagging-based ensemble approach outperformed all other models, achieving an R^2 of 0.934 and an RMSE of 2.037 on unseen test data. The minimal deviation of 0.007 in the test R^2 score from the training data indicated that the Bagging model is more robust and generalizes better than DT and AdaBoost. Thus, the success of the optimized Bagging model framework, with predictions of effectiveness within a 2.03 RMSE margin across the 9 to 51.96 range, can replace the traditional approach with a dynamic model that predicts in real time without losing physical grounding. Further, SHAP-based analysis is integrated to bridge the gap between the data-driven ML model and thermodynamic principles. The SHAP analysis confirmed that the cold flow rate is the primary input for generating effectiveness, with an inverse relationship. This is consistent with residence-time theory and convective heat transfer coefficients. The results establish that RSM-BBD is valuable for identifying specific optimal operating points, and the Bagging-based ML framework offers a more generalized and robust tool for real-time performance prediction. The proposed hybrid approach of optimization and prediction offers a robust and efficient framework, which can guide future operational enhancements and contribute to the development of smart building technologies

Author Contributions

N. Mohammed planned the scheme, initiated the work, and suggested the experiments, performed formal analysis and investigation; F. Ahmed conducted the experiments and analyzed the empirical results; H. Mewada developed the mathematical modeling, ML model implementation, and examined the software validation. The manuscript was written through the contribution of all authors. All authors discussed the results, reviewed, and approved the final version of the manuscript.

Acknowledgments

Not applicable.

Conflict of Interest

The authors declared no potential conflicts of interest concerning the research, authorship, and publication of this article.

Funding

The authors received no financial support for the research, authorship, and publication of this article.

Data Availability Statements

The datasets generated and/or analyzed during the current study are available from the corresponding author on reasonable request.

References

[1] Ahmed, F., Sharizal Abdul Aziz, M., Palaniandy, P., Shaik, F., A review on application of renewable energy for desalination technologies with emphasis on concentrated solar power, *Sustainable Energy Technologies and Assessments* 53, 2022, 102772.
[2] Indumathy, M., Sobana, S., Panda, B., Panda, R.C., Modelling and control of plate heat exchanger with continuous high-temperature short time milk pasteurization process – A review, *Chemical Engineering Journal Advances*, 11, 2022, 100305.
[3] Zheng, D., Wang, J., Chen, Z., Baleta, J., Sundén, B., Performance analysis of a plate heat exchanger using various nanofluids, *International Journal of Heat and Mass Transfer*, 158, 2020, 119993.
[4] Alazwari, M.A., Abu-Hamdeh, N.H., Salilih, E.M., Exergetic performance analysis on helically coiled tube heat exchanger-forecasting thermal conductivity of SiO2/EG nanofluid using ANN and RSM to examine effectiveness of using nanofluids, *Journal of Thermal Analysis and Calorimetry*, 144, 2021, 2721–2733.
[5] Yoladi, M., Akyurek, E.F., Kotcioglu, İ., Experimental investigation of cross-flow heat exchangers with helical fins: Performance analysis via RSM and ANN, *International Journal of Thermal Sciences*, 218, 2025, 110111.
[6] Gherasim, I., Taws, M., Galanis, N., Nguyen, C.T., Heat transfer and fluid flow in a plate heat exchanger, Part I. Experimental investigation, *International Journal of Thermal Sciences*, 50, 2011, 1492–1498.
[7] Zeinali Heris, S., Pasvei, S., Pourpasha, H., Mohammadfam, Y., Sharifpur, M., Meyer, J., Experimental analysis of graphene-COOH/water and TiO2/Water nanofluids in plate heat exchangers: Heat transfer performance and stability, *Renewable Energy*, 245, 2025, 122822.
[8] Tekir, M., Experimental study on the thermal performance of hybrid nanofluid in a compact plate heat exchanger under the influence of a magnetic field, *Case Studies in Thermal Engineering*, 69, 2025, 106031.
[9] Yahaya, R.I., Mustafa, M.S., Md Arifin, N., Md Ali, F., Mohamed Isa, S.S.P., Heat transfer optimization for the unsteady mixed convection flow of hybrid nanofluid over a permeable EMHD riga plate with thermal radiation and convective boundary condition, *Multiscale and Multidisciplinary Modeling, Experiments and Design*, 8, 2025, 192.
[10] Lowrey, S., Hughes, C., Sun, Z., Thermal-hydraulic performance investigation of an aluminum plate heat exchanger and a 3D-printed polymer plate heat exchanger, *Applied Thermal Engineering*, 194, 2021, 117060.
[11] Ham, J., Lee, G., Kwon, O., Bae, K., Cho, H., Numerical study on the flow maldistribution characteristics of a plate heat exchanger, *Applied Thermal Engineering*, 224, 2023, 120136.
[12] Mayer, J.M., Walters, N., Albrecht, K.J., Madden, D.A., Bala Chandran, R., Experimental characterization of heat transfer coefficients in a moving-bed shell-and-plate heat exchanger with non-contact temperature measurements, *International Journal of Heat and Mass Transfer*, 242, 2025, 126819.
[13] Ben Hamida, M.B., Ali, A.B.M., Sawaran Singh, N.S., Mostafa, L., Optimization of MXene-based aqueous ionic liquids for solar systems using conventional and AI-based techniques, *Scientific Reports*, 15, 2025, 20565.
[14] Ham, J., Lee, G., Kwon, O., Bae, K., Cho, H., Numerical study on the flow maldistribution characteristics of a plate heat exchanger, *Applied Thermal Engineering*, 224, 2023, 120136.
[15] Gut, J.A.W., Pinto, J.M., Optimal configuration design for plate heat exchangers, *International Journal of Heat and Mass Transfer*, 47, 2004, 4833–4848.
[16] He, S., Wang, M., Forgione, N., Pucciarelli, A., Tian, W.X., Qiu, S.Z., Su, G.H., A multi-task Transformer-Mamba-Seq framework for real-time estimation of spatiotemporal thermal stratification in passive residual heat exchanger, *International Communications in Heat and Mass Transfer*, 169, 2025, 109868.
[17] Kanaris, A.G., Mouza, A.A., Paras, S.V., Optimal design of a plate heat exchanger with undulated surfaces, *International Journal of Thermal Sciences*, 48, 2009, 1184–1195.
[18] Elbarghthi, A.F.A., Dvorak, V., Al-Dailami, Z., Bediako, E.G., Wen, C., Multi-domain analysis and optimisation for plate heat exchangers: Integrating theory, Experiment, and CFD-based approaches, *Energy Conversion and Management*, 344, 2025, 120187.
[19] Mikhaeil, M., Gaderer, M., Dawoud, B., On the development of an innovative adsorber plate heat exchanger for adsorption heat transformation processes; an experimental and numerical study, *Energy*, 207, 2020, 118272.
[20] Zou, J., Hirokawa, T., An, J., Huang, L., Camm, J., Recent advances in the applications of machine learning methods for heat exchanger modeling—a review, *Frontiers in Energy Research*, 11, 2023.
[21] Yoladi, M., Akyurek, E.F., Kotcioglu, İ., Experimental investigation of cross-flow heat exchangers with helical fins: Performance analysis via RSM and ANN, *International Journal of Thermal Sciences*, 218, 2025, 110111.
[22] He, S., Ye, Y., Wang, M., Zhang, J., Tian, W., Qiu, S., Su, G.H., A machine learning and CFD based approach for fouling rapid prediction in shell-and-tube heat exchanger, *Nuclear Engineering and Design*, 432, 2025, 113759.
[23] Yang, Z., He, S., Yu, J., Wang, Q., Qiu, H., Wang, M., Tian, W., Su, G.H., A machine learning-based generative design approach for rapid topology optimization of microchannel heat sinks, *International Communications in Heat and Mass Transfer*, 169, 2025, 109655.
[24] Ahmed, F., Aziz, M.S.A., Shaik, F., Khor, C.Y., Optimization of a novel spray flash desalination system integrated with concentrated solar power utilizing response surface methodology, *Desalination*, 558, 2023, 116640.
[25] Sun, Y., Cai, L., Chen, Y., Wang, S., Optimization of a high through-flow design turbine using response surface method, *Physics of Fluids*, 36, 2024, 046106.
[26] He, Y., Rao, L., E, D., Lai, N.-C., Fang, J., Jiang, Z., Multi-response optimization for a waste heat recovery rotary drum with flights: Focusing on enhancement and homogenization of heat exchange, *Chemical Engineering Research and Design*, 218, 2025, 218–229.
[27] Mohammed, N., Palaniandy, P., Shaik, F., Deepanraj, B., Mewada, H., Statistical analysis by using soft computing methods for seawater biodegradability using ZnO photocatalyst, *Environmental Research*, 227, 2023, 115696.
[28] Xu, L., Wang, B., Zhang, Y., Wu, R., Liu, J., Li, X., Impact damage prediction of steel tube confined reinforced concrete columns based on a finite Element–machine learning model and transfer learning ideas, *Journal of Building Engineering*, 113, 2025, 114008.
[29] Liu, K., Lu, C., Chen, W., Chen, B., Dai, Y., A machine learning framework for predicting the fire resistance time of cold-formed steel walls, *Journal of Building Engineering*, 2025, 114206.
[30] Mihalakakou, G., Giannadakis, A., Malefaki, S., Souliotis, M., Georgiou, P., Romaios, A., Antzoulatou, A., Nikolakopoulos, P., Paravantis, J.A., Coupling simulation-based and machine learning methodologies for energy optimization and environmental impact mitigation in buildings, *Journal of Building Engineering*, 112, 2025, 113809.
[31] Zhou, S., Sun, Z., Li, W., Guo, J., Sun, D., Xu, L., Wu, K., A Hybrid Machine Learning Framework with GAN-Based Data Augmentation for Predicting Strain Properties of Fiber-Reinforced Repair Mortar, *Journal of Building Engineering*, 2025, 114140.
[32] Shehzad, A., Xiu-Xin, W., Xing-Huai, H., Ullah, K., Mohammad, A., Althobaiti, A., Flah, A., AI-driven seismic optimization of outrigger systems in high-rise buildings: A machine learning framework for enhanced performance in earthquake-prone regions, *Journal of Building Engineering*, 112, 2025, 113864.
[33] Baruah, A.C., Sychterz, A.C., Machine learning-based damage classification and comparative life cycle assessment of Origami Pill Bug for emergency shelters, *Journal of Building Engineering*, 113, 2025, 114051.

ORCID iD

Nayeemuddin Mohammed https://orcid.org/0000-0002-7757-936X
Faizan Ahmed https://orcid.org/0000-0002-4792-2139
Hiren Mewada https://orcid.org/0000-0002-3579-8708

How to cite this article: Nayeemuddin M., Ahmed F., Mewada H. Machine Learning Modeling and Experimental Optimization of Heat Exchanger for Efficient Building Systems, *J. Appl. Comput. Mech.*, xx(x), 2026, 1–13. https://doi.org/10.22055/jacm.2026.49121.5747